An *LLC*-DAB Bidirectional DCX Converter With Wide Load Range ZVS and Reduced Switch Count

Yuefeng Liao, *Student Member, IEEE*, Guo Xu, *Senior Member, IEEE*, Tao Peng, *Member, IEEE*, Yao Sun, *Member, IEEE*, Dong Liu, *Senior Member, IEEE*, Yongheng Yang, *Senior Member, IEEE*, and Mei Su

***Abstract*—An *LLC* dual active bridge (DAB) bidirectional converter with reduced switch count as a dc–dc transformer (DCX) is proposed in this article. It can achieve voltage regulation, full load range zero voltage switching (ZVS) for eight main switches and wide load range ZVS for four auxiliary switches, with consideration of the switch junction capacitors under different power direction. A part portion of total power is transferred through an auxiliary DAB circuit to achieve voltage regulation and bidirectional power conversion. The main power is transferred through *LLC* circuit with an easy PWM scheme achieving high conversion efficiency. Different from the existing *LLC*-DAB DCX structure, the two secondary side transformer outputs are in parallel, and connected to the same full-bridge circuit. In this way, the auxiliary DAB circuit can not only adjust the output voltage, but also can inject current into the secondary side to help achieving ZVS of switches without synchronous rectifier circuit. The converter operation principle is analyzed under different power directions, and ZVS is analyzed with the consideration of all the switch junction capacitors. Based on the analysis, the design consideration is introduced. Finally, a 2-kW prototype with 750 V input and 400 V output is built up to verify the effectiveness of the proposed solution.**

***Index Terms*—Bidirectional power flow, *LLC*-DAB bidirectional converter, zero voltage switching.**

I. Introduction

IN RECENT years, due to the high efficiency, wide range of zero voltage switching (ZVS) and electrical isolation, *LLC* resonant converter is widely used in energy storage system [1], the electric vehicles [2], and solid state transformers [3].

Manuscript received December 21, 2020; revised March 26, 2021 and June 24, 2021; accepted August 10, 2021. Date of publication August 18, 2021; date of current version October 15, 2021. This work was supported in part by the National Natural Science Foundation of China under Grant 51907206, in part by the National Natural Science Foundation of China under Grant 61933011, in part by the Major Project of Changzhutan Self-Dependent Innovation Demonstration Area under Grant 2018XK2002, and in part by the Project of Innovation-driven Plan in Central South University under Grant 2019CX003. Recommended for publication by Associate Editor S. K. Mishra. *(Corresponding author: Guo Xu.)*

Yuefeng Liao, Guo Xu, Yao Sun, and Mei Su are with the School of Automation, Central South University, Changsha 410083, China, and also with the Hunan Provincial Key Laboratory of Power Electronics Equipment and Grid, Changsha 410083, China (e-mail: liaoyuefeng_uav@126.com; xuguocsu@csu.edu.cn; yaosuncsu@gmail.com; sumeicsu@csu.edu.cn).

Tao Peng is with the School of Automation, Central South University, Changsha 410083, China (e-mail: pandtao@csu.edu.cn).

Dong Liu is with the Department of Electronic and Electrical Engineering, University of Sheffield, Sheffield S1 3JD, U.K. (e-mail: liudong@ieee.org).

Yongheng Yang is with the College of Electrical Engineering, Zhejiang University, Hangzhou 310027, China (e-mail: yang_yh@zju.edu.cn).

Color versions of one or more figures in this article are available at https://doi.org/10.1109/TPEL.2021.3105828.

Digital Object Identifier 10.1109/TPEL.2021.3105828

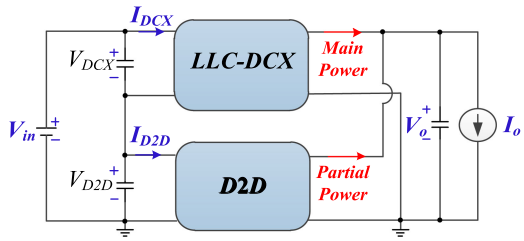

Fig. 1. General structure of the sigma converter. DCX means dc–dc transformer and D2D means dc to dc converter.

Using an *LLC* converter as a dc–dc transformer (DCX) [4], [5], which operates at the resonant frequency, is a suitable solution for maximizing the conversion efficiency. However, the voltage regulation capability cannot be maintained because the switching frequency is fixed [6], [7]. To make the DCX converter achieve both flexible voltage regulation and high efficiency conversion, the sigma converter structure first proposed in [8] can be utilized. In [9], a 1-V voltage regulation module using sigma structure is introduced. It is a combination of an *LLC*-DCX converter and a dc to dc (D2D) converter (like a buck converter), which are series-connected at the input and parallel-connected at the output (ISOP), as shown in Fig. 1. This structure is suitable for applications that need to connect high voltage interface with low voltage interface, where the high-voltage port has exceeded the withstand voltage of a single switching device, such as railway traction systems, new energy electric vehicle charging systems, and energy router [10]. With this sigma structure, the inputs of multiple dc–dc modules can be connected in series to solve the disadvantage of the conventional single converter with limited voltage stress and power flow. Similar to this structure, in [11] and [12], a regulated *LLC*-DCX is proposed. An auxiliary pulsewidth modulation (PWM) dc–dc stage is used to regulate the output voltage. In these cases, *LLC*-DCX converter works at the resonant frequency and transfers the main power to achieve high efficiency conversion, and the D2D converter is used to maintain the voltage regulation through partial transferring power. It is worth pointing out that, for these studies in [9]–[12], the power is unidirectional because the added D2D converter for adjusting the output voltage is unidirectional. Meanwhile, the ZVS operation is easy to achieve for *LLC* converter in the sigma structure, as the primary side bridge can work as a high frequency inverter and the

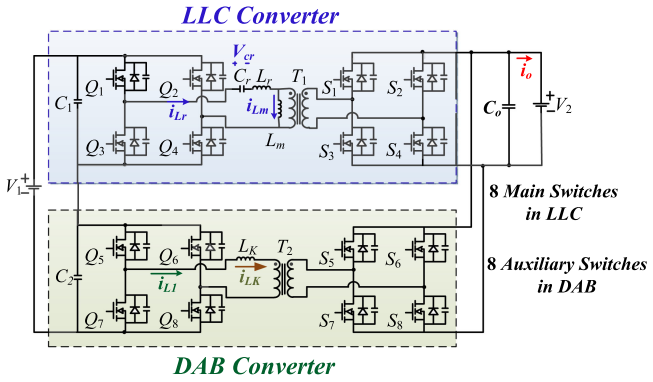

Fig. 2. Traditional DAB-*LLC* DCX converter structure proposed in [17].

secondary side bridge can work as a synchronous rectifier (SR) in unidirectional application [9]. To make the sigma converter capable of transferring bidirectional power with isolation, the D2D converter can be replaced by an isolated bidirectional converter.

For bidirectional power transferring, the dual active bridge (DAB) converter is a preferred topology with a wide range of ZVS operation. For a DAB converter, the control of the power flow and direction is simple because the power is directly related to the phase shift angle [13], [14]. In [15], it is mentioned that DAB converter has higher efficiency than *LLC* converter under heavy load, but such a conclusion is obtained in high-step-down fixed-conversion-ratio applications, where the current is relatively large being the main efficiency-limiting factor. However, for high voltage and low current occasions, the current is only one of the key factors affecting efficiency, as well as circulating current, ZVS and etc. [16]. It is worth noting that the D2D converter only transfers a part portion of the total power in the sigma structure, thus, these shortcomings can be minimized to some extent. Consequently, to utilize both the bidirectional power flow capability of DAB converter and high efficiency of *LLC*-DCX converter, a hybrid modular DCX utilizing a series-resonant-DAB (SR-DAB) and phase-shift-DAB (PS-DAB) converter topology is studied in [17], which can also be regarded as a sigma structure. In [18], a hybrid dc transformer with the ISOP configuration is proposed combining multiple series resonant converters and DAB converters. It is then used to be an interface between medium voltage dc and low voltage dc distribution grids. In addition, *LLC* converter and DAB converter are combined in [19] to form a DAB-*LLC* DCX converter, as shown in Fig. 2. With properly design, the main power flows through *LLC* converter, and DAB converter can undertake only a part portion of power to adjust the output voltage. In this way, the high efficiency conversion of *LLC* converter and the natural bidirectional power control capability of DAB converter can be fully utilized [19]. However, these studies [17]–[19] mainly focus on the power control for the sigma connection utilizing multitypes of converters, while the PWM scheme and the ZVS operation are not further investigated. In addition, due to the combination of multiple converters, the switch count becomes significantly large, resulting in more losses if the ZVS operation cannot be ensured.

For a full load range ZVS of *LLC* converter in DAB-*LLC* structure under unidirectional power transfer, as mentioned previously, it is easily achieved since the secondary side switches only operate as a SR according to the current zero crossing point. However, for bidirectional power transmission applications, the PWM scheme for *LLC* converter is a challenge, because the SR circuit would have to exchange under different power transmission direction. In [20], a PWM strategy is proposed to face with bidirectional power transfer without power flow detection procedures, but only switches in one bridge can achieve ZVS. Similarly, although the switches can be turned on and off simultaneously at the primary and secondary side without SR detection and achieve constant voltage gain, only half of the switches can achieve ZVS operation [21]. At the same time, it is analyzed in [22] that when the switching frequency equals to the resonant frequency, if the drive signals of primary and secondary side are consistent, the secondary side is hard to achieve soft switching. To achieve the full load range ZVS operation of all switches, the series-resonant converter is modified with an auxiliary inductor in [23]. However, the added auxiliary inductor will increase the circuit complexity and induce additional losses. In [24], a digital adaptive synchronous rectification driving scheme is proposed to achieve ZVS operation of all switches. And, a bidirectional *LLC* converter, which achieving transition between the forward and backward mode is presented in [25]. However, for these strategies [24], [25], the PWM logics shifting under different power transmission directions are complicated, and are highly dependent on the system parameters. In addition, the effects of junction capacitors on the ZVS operation are not discussed for these previous methods. As pointed out in [26], the secondary side junction capacitors can cause the inconsistent charge/discharge time. This further increases the complexity of achieving full load range ZVS achievement.

To achieve full load ZVS range of *LLC* converter in the sigma structure, this article proposes an *LLC*-DAB bidirectional DCX converter with reduced switch count. The junction capacitors of all the switches are considered when analyze the working principle and ZVS achievement. The connection of *LLC* and DAB in the sigma structure is reconstructed. Under the proposed modification, four switches in the secondary side can be removed, and it also offers a new solution for the bidirectional *LLC* converter to achieve the full load range ZVS operation of all switches. The secondary side of DAB transformer is directly connected in parallel with the secondary side of *LLC* transformer to provide sufficient charging energy to achieve the ZVS operation of the secondary side switches. It should be pointed out that DAB circuit only transfers part portion of the total power and it can achieve wide load range ZVS when the voltage gain variation is small. The advantages of the proposed solutions are summarized as follows.

1) The output voltage can be regulated while ensuring high efficiency. Referring to the sigma structure, the proposed converter consists of a bidirectional *LLC* circuit and an auxiliary DAB circuit. The main power flows through *LLC* primary circuit, and the auxiliary DAB circuit is used

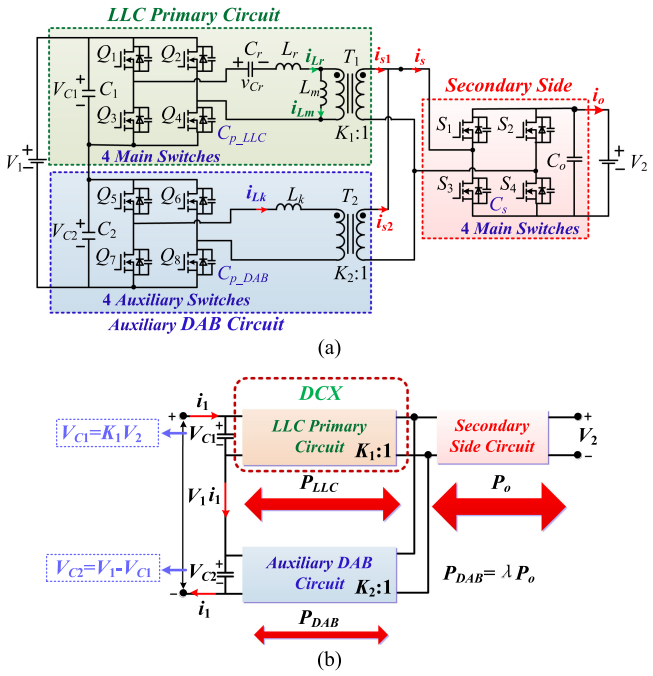

Fig. 3. Proposed *LLC*-DAB bidirectional DCX converter. (a) Detailed circuit diagram. (b) Power distribution diagram.

to control the power flow direction. And when the input voltage varies, the output voltage can be regulated.

2) The switch count of the secondary side is reduced from 8 to 4, and the auxiliary DAB circuit can not only transfer partial power to adjust its output voltage, but also can inject current into the secondary side to support the ZVS operation.
3) The PWM scheme is easy to be implemented. Under different power transmission directions, without changing the modulation logics of *LLC* primary circuit and the secondary side, whose driving signals of the primary and secondary sides are identical, full load range ZVS can be achieved for the main eight power switches, and four auxiliary switches in auxiliary DAB circuit can achieve wide ZVS range. This simple control method does not require power transmission direction judgment and SR detection.

The rest of this article is organized as follows. Section II introduces the topology and analyzes the operation modes under different power directions. The analysis of ZVS range for all the switches under different power directions is presented in Section III, Section IV gives the parameters design, and Section V illustrates the experimental results from a 2 kW prototype, which verify the effectiveness of the proposed topology. Finally, Section VI concludes this article.

II. Proposed Converter and Operation Principles

A. Converter Topology

The topology of the proposed *LLC*-DAB bidirectional DCX converter is shown in Fig. 3(a). Different from the structure shown in Fig. 2, the secondary side of the transformer of auxiliary DAB circuit is directly connected in parallel with the secondary side of the transformer of *LLC* primary circuit. In this way, only four switches are needed in secondary side, which reduces the switch count.

In Fig. 3(a), Q_1–Q_4, Q_5–Q_8 are the switches of *LLC* primary circuit and auxiliary DAB, respectively. S_1–S_4 are the secondary side switches. L_r, L_m, and L_k are the resonant inductor, magnetizing inductor, and leakage inductor, respectively. C_o, C_1, C_2, and C_r are the output filter capacitor, and input capacitor of *LLC* primary circuit, input capacitor of auxiliary DAB circuit and resonant capacitor, respectively. $C_{p\text{-}LLC}$, $C_{p\text{-}\mathrm{DAB}}$, and C_s denote the junction capacitors for switches in *LLC* primary circuit, auxiliary DAB circuit and secondary side, respectively, which are equivalently obtained according to [27]. V_1, V_2, V_{C1}, V_{C2}, and v_{Cr} represent the total input voltage, output voltage, input voltage of *LLC* primary circuit, input voltage of auxiliary DAB circuit and resonant capacitor voltage, respectively. i_s, i_{Lr}, i_{Lm}, and i_{Lk} are the secondary side current, resonant current, magnetizing inductor current, and leakage current, respectively. K_1 and K_2 are the turns ratio for transformers T_1 and T_2, respectively. With proper design of these two turns ratios, the distribution of the power for *LLC* primary circuit and auxiliary DAB circuit can be controlled. It is assumed that $V_{C1}/K_1 = V_2$ under the steady state since *LLC* circuit works in DCX mode. The main power flows through *LLC* primary circuit to achieve high conversion efficiency, and the auxiliary DAB circuit utilizes partial power to achieve voltage regulation and bidirectional power flow control, as shown in Fig. 3(b), where λ is the power distribution coefficient. Under this power distribution, Q_1–Q_4 and S_1–S_4 are selected as main switches and Q_5–Q_8 are selected as auxiliary switches.

The PWM logics are shown in Fig. 4, where T_s is the switching period. The proposed converter is operated at a fixed resonant switching frequency with 50% duty cycle. The upper switch and lower switch in any bridge leg are complementary. The driving signals of Q_i ($i = 1, 2, 3,$ and 4) are the same as that for S_i ($i = 1$, 2, 3, and 4) at the secondary side. For the auxiliary DAB circuit, Q_5 and Q_8 are turned ON and OFF simultaneously, and has a phase shift angle ϕ with respect to the driving signal of Q_1 and S_1. The voltage regulation and power flow control can be obtained with the controlling of ϕ. It is worth noting that the power transfer from V_1 side to V_2 side is denoted as forward power transfer. Fig. 4 shows the key waveforms of the proposed converter under forward and backward power transmission mode.

B. Forward Power Transmission Mode

Fig. 4(a) shows the key waveforms under forward power transmission mode. The equivalent circuits during each time interval are shown in Fig. 5.

Before t_0, the switches of *LLC* primary circuit and the secondary side are turned off. And, Q_5 and Q_8 are conducted. The resonant current i_{Lr} flows through the body diodes of Q_1 and Q_4. The secondary side current i_s flows through the body diodes of S_1 and S_4, as shown in Fig. 5(a).

Stage 1 [t_0, t_1] [see Fig. 5(b)]: At t_0, Q_1, Q_4, S_1, and S_4 are turned ON with zero voltage switching. *LLC* primary circuit

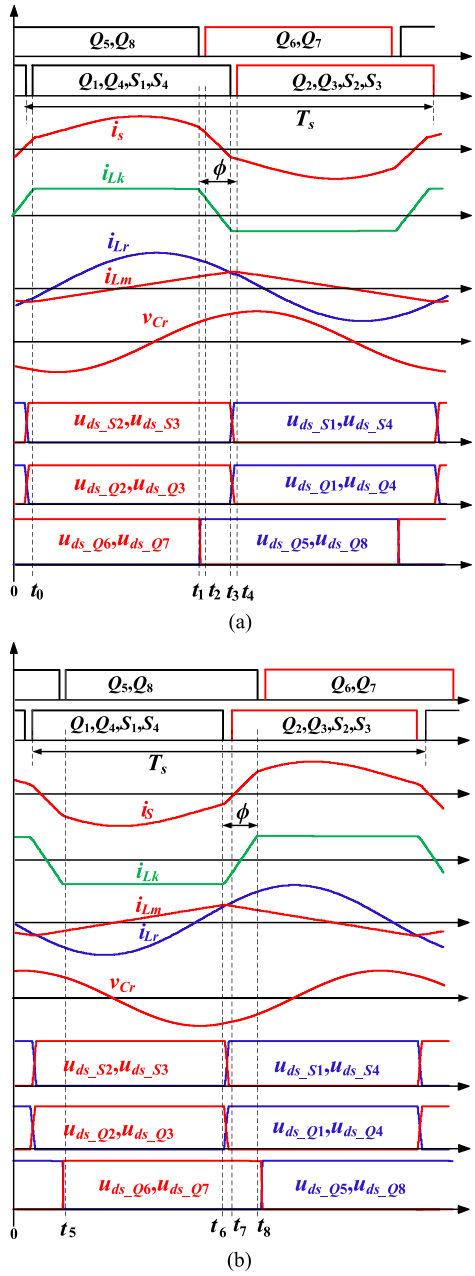

Fig. 4. Key waveforms of the proposed converter. (a) Forward power transmission mode. (b) Backward power transmission mode.

enters the resonance process. The resonant current i_{Lr}, magnetizing current i_{Lm}, leakage current i_{Lk}, and resonant capacitor voltage v_{Cr} can be expressed as

$$\begin{cases} i_{Lr}(t) = \sqrt{\left(\frac{v_{Cr}(t_0)}{Z_0}\right)^2 + i_{Lr}(t_0)^2}\sin\left[\omega_r(t-t_0)-\theta\right] \\ i_{Lm}(t) = \frac{K_1V_2}{L_m}t - \frac{K_1V_2T_s}{4L_m} \\ i_{Lk}(t) = i_{Lk}(t_0) + \frac{V_{C2}-K_2V_o}{L_k}(t-t_0) \\ v_{Cr}(t) = v_{Cr}(t_0) - \frac{1}{C_r}\int_{t_0}^{t} i_{Lr}(t)\,dt \end{cases} \tag{1}$$

where Z_0 is the impedance of resonant tank. The relationship between i_s and the currents of the two transformer secondary

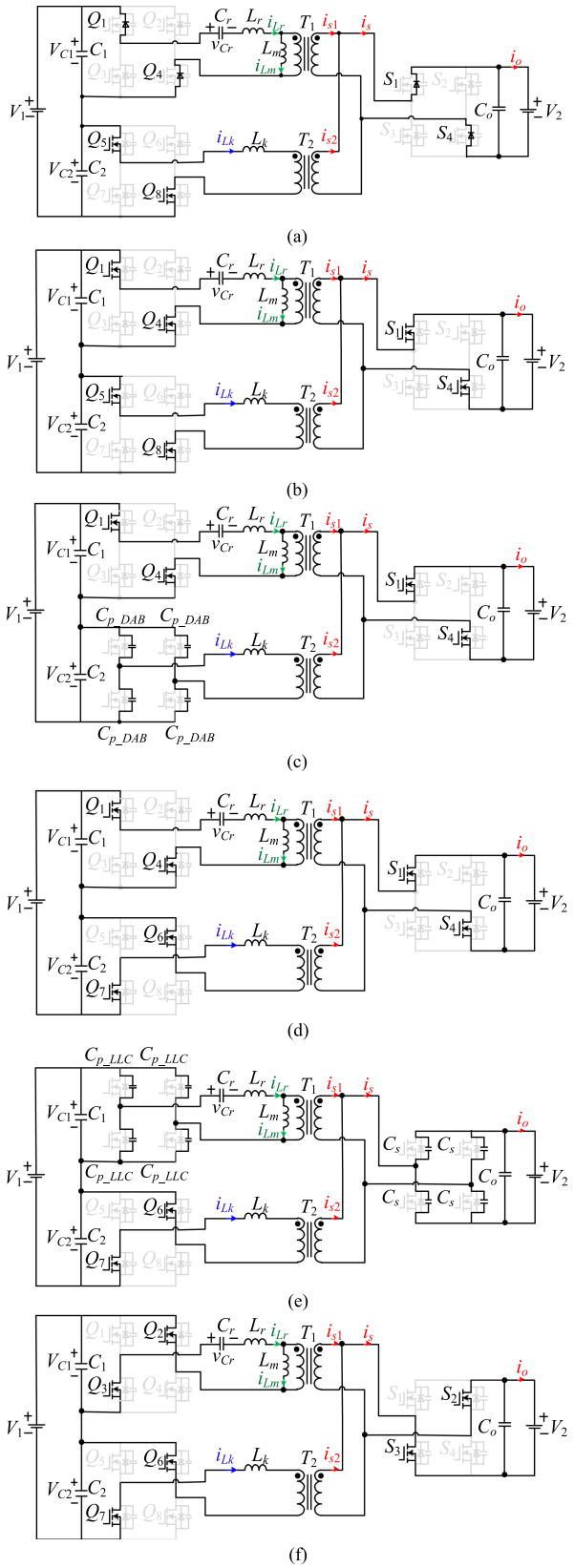

Fig. 5. Equivalent circuit of the proposed converter in forward power transmission mode. (a) Before t_0. (b) $[t_0, t_1]$. (c) $[t_1, t_2]$. (d) $[t_2, t_3]$. (e) $[t_3, t_4]$. (f) After t_4.

sides (i_{s1} and i_{s2}), is shown as follow:

$$i_s = i_{s1} + i_{s2} = K_1 (i_{Lr} - i_{Lm}) + K_2 i_{Lk}. \tag{2}$$

Stage 2 [t_1, t_2] [see Fig. 5(c)]: At t_1, Q_5 and Q_8 are turned OFF. The leakage current $i_{Lk}(t_1)$ is larger than zero, which is expressed as

$$i_{Lk}(t_1) = \frac{2K_2V_2\phi - K_2V_2 + V_{C2}}{4L_k f_s} = \frac{K_2V_2\phi}{2L_k f_s} \tag{3}$$

where f_s is the switching frequency. The junction capacitors of auxiliary DAB circuit can be discharged/charged through i_{Lk}. At the end of this stage, i_{Lk} flows through the body diodes of Q_6 and Q_7 to create the ZVS turn ON condition.

Stage 3 [t_2, t_3] [see Fig. 5(d)]: At t_2, Q_6 and Q_7 are turned ON with zero voltage switching. Then, i_{Lk} starts to decrease with a constant slop.

Stage 4 [t_3, t_4] [see Fig. 5(e)]: At t_3, Q_1, Q_4, S_1, and S_4 are OFF. At this time, i_{Lr} is equal to i_{Lm}, which can be expressed as

$$i_{Lr} = i_{Lm} = \frac{K_1V_2}{4L_m f_s}. \tag{4}$$

During this stage, the magnetizing inductor current will charge/discharge the junction capacitors of switches in *LLC* primary circuit. As for the secondary side switches, even though the secondary side current of T_1 will approach zero, the current of T_2 can still provide energy to discharge/charge the junction capacitor of the secondary side switches to achieve ZVS switching. The current of the transformer secondary side can be expressed as (5). At the end of this stage, the body diodes of Q_2, Q_3, S_2, and S_3 will be conducted

$$i_s(t_3) = i_{s2}(t_3) = K_2 i_{Lk} < 0. \tag{5}$$

Stage 5 [*After* t_4] [see Fig. 5(f)]: At t_4, Q_2, Q_3, S_2, and S_3 turn ON with zero voltage. After t_4, the operation mode is similar to *Stage* 1, and the other half of the switching period begins.

C. Backward Power Transmission Mode

When the power transfer is reversed, the phase-shift angle ϕ will be negative. The backward operation is shown in Fig. 4(b).

Stage 1 [t_5, t_6] [see Fig. 6(a)]: At t_5, Q_5 and Q_8 are turn ON. During this stage, L_r is resonating with C_r, and i_{Lk} increases linearly since the applied voltage is constant.

Stage 2 [t_6, t_7] [see Fig. 6(b)]: At t_6, Q_1, Q_4, S_1, and S_4 are turned OFF. And, i_{Lr} equals to i_{Lm}. At this time, $i_s = i_{s2}$, since i_{s1} is approaching zero.

Then, the junction capacitors of switches in *LLC* primary circuit can be charged/discharged by current i_{Lr}, and those in the secondary side can be charged/discharged by current i_{s2}. At the end of this stage, the body diodes of Q_2, Q_3, S_2, and S_3 will be conducted.

Stage 3 [t_7, t_8] [see Fig. 6(c)]: At t_7, Q_2, Q_3, S_2, and S_3 are ON with zero voltage. Then, i_{Lk} starts to increase and the resonant tank enters into the resonance process again.

Stage 4 [*After* t_8] [see Fig. 6(d)]: At t_8, Q_5 and Q_8 are turned OFF. The discharge/charge process of junction capacitor is similar to the forward operation. After t_8, the operation modes are similar with the previous stage.

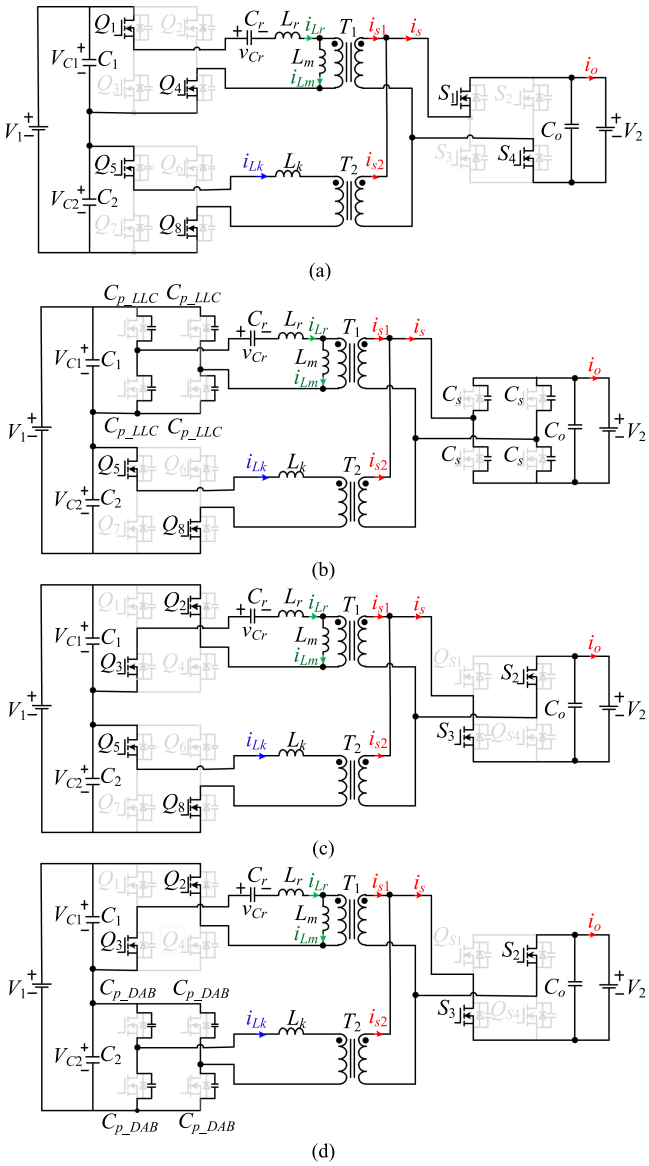

Fig. 6. Equivalent circuit of the proposed converter in backward power transmission mode. (a) [t_5, t_6]. (b) [t_6, t_7]. (c) [t_7, t_8]. (d) After t_8.

III. ZVS Operation Analysis

This section mainly analyzes ZVS conditions of all the switches under the forward power transmission and backward power transmission modes.

A. ZVS Analysis of the Secondary Side Circuit

A. 1) Forward Power Transmission Mode: As analyzed previously, i_{Lk} reaches the negative maximum during *Stage* 4 in the forward power transmission mode, which can inject current to the secondary side to assist the discharge/charge process according to (5). Moreover, when the junction capacitors of *LLC* primary circuit complete discharge/charge process, i_{Lr} starts to decrease. The difference between i_{Lr} and i_{Lm} can also assist the secondary side to achieve the ZVS operation. Then, to completely discharge/charge of secondary side junction capacitors

before the end of the dead time, the following relationship should be satisfied:

$$2K_2 i_{Lk}(t_3) T_{\text{dead}} + (T_{\text{dead}} - T_{p\_\text{dis}}) K_1 i_{Lm}(t_3) \geq 4C_s V_2 \tag{6}$$

where $i_{Lk}(t_3)$ and $i_{Lm}(t_3)$ can be calculated according to (1), and T_{dead} and T_{p_dis} are dead time and discharge/charge time of *LLC* primary junction capacitors, respectively.

2) Backward Power Transmission Mode: Under the backward power transmission mode, the secondary side current can be deduced from the circuit

$$i_s = K_1 (i_{Lr} - i_{Lm}) + K_2 i_{Lk}. \tag{7}$$

The difference of the ZVS operation analysis between the backward and forward power transmission mode is that the transformer secondary current of auxiliary DAB circuit starts to decrease toward zero, as shown in Fig. 4(b). Then, the secondary side current at the end of the discharge/charge process can be expressed as

$$\begin{aligned} i_{s\_\text{end}} = {} & K_1 (i_{Lr}(t_6) + \Delta i_{Lr} - i_{Lm}(t_6)) \\ & + K_2 (i_{Lk}(t_6) + \Delta i_{Lk}) \end{aligned} \tag{8}$$

where Δi_{Lr} is the variation of resonant current caused by the inconsistent discharge/charge time of C_{p_LLC} and C_s, and Δi_{Lk} means the current injected into the secondary side by auxiliary DAB circuit gradually decreases. According to (8), the range of ZVS operation of the secondary side is narrower.

In order to ensure the achievement of ZVS operation of the secondary side, the secondary side current needs to be negative at end of *Stage* 2 $[t_6, t_7]$ in the backward power transmission mode. As the switches are turned off at the resonant point, $i_{Lr}(t_6)$ equals to $i_{Lm}(t_6)$ in (8). Thus, the secondary side current at the end of this interval i_{s_end} can be expressed as

$$\begin{aligned} & i_{s\_\text{end}} \\ & = K_1 \Delta i_{Lr} - \frac{K_2{}^2 V_2 \phi}{2L_k f_s} + K_2 \frac{V_{C2} + K_2 V_2}{L_k} (T_{\text{dead}} - T_{\text{dis}}) \end{aligned} \tag{9}$$

where T_{dis} is the total discharge/charge time of primary and secondary. The difference of the discharge/charge time for primary and secondary side junction capacitors will bring a sudden change on the voltage v_{Lr} crossing the resonant inductor L_r, thus changing the sign of Δi_{Lr}. When the discharge/charge time of the secondary side is shorter than *LLC* primary circuit $v_{Lr} = V_{C1} + K_1 V_2 + v_{Cr}$, which make Δi_{Lr} to be positive. Conversely, if the discharge/charge time of the secondary side is longer than *LLC* primary circuit $v_{Lr} = -V_{C1} - K_1 V_2 + v_{Cr}$, which make Δi_{Lr} to be negative. According to (9), the range of ZVS operation can be extended if Δi_{Lr} is negative. Therefore, T_{p_dis} is designed smaller than the discharge/charge time of the secondary side T_{s_dis} to make v_{Lr} smaller than zero in this article. The theoretical discharge/charge time can be calculated as

$$\begin{cases} T_{p\_\text{dis}} = 8C_{p\_LLC} L_m f_s \\ T_{s\_\text{dis}} = \dfrac{4C_s L_k f_s}{K_2{}^2 \phi}. \end{cases} \tag{10}$$

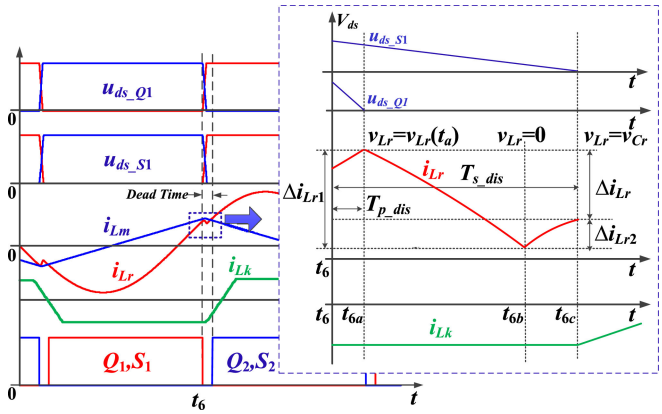

Fig. 7. Illustration of the discharge/charge process under backward power transmission mode.

An illustration of the discharge/charge process is shown in Fig. 7. The equivalent charging capacitor value is used here, so the discharge/charge process can be linear. Then, v_{Lr} at the end of the discharge/charge time of *LLC* primary circuit, can be calculated as

$$\begin{aligned} v_{Lr}(t_{6a}) &= -2K_1 V_2 + v_{Cr}(t_{6a}) + \frac{T_{p\_\text{dis}} K_1 K_2 i_{Lk}(t_6)}{C_s} \\ &= -2K_1 V_2 + \frac{V_2}{4RC_r f_s (K_1 + K_2)} + \frac{T_{p\_\text{dis}} K_1 K_2{}^2 V_2 \phi}{2L_k f_s C_s} < 0 \end{aligned} \tag{11}$$

where R denotes the load. Since the discharge/charge process of secondary side is not complete, the remaining discharge/charge time is divided into two interval from t_{6a} to t_{6c}.

The first duration is from t_{6a} to the time when v_{Lr} becomes zero at t_{6b}, and i_{Lr} will decrease to be less than i_{Lm}, which causes the current of the transformer secondary side of *LLC* primary circuit i_{s1} less than zero. Then, the discharge/charge process of the secondary side will be accelerated. Denoting that $T_{6ba} = t_{6b} - t_{6a}$, it is obtained that

$$\begin{aligned} v_{Lr}(t_{6b}) = v_{Lr}(t_{6a}) & - \frac{K_1 K_2{}^2 V_2 \phi}{2C_s L_k f_s} \\ & + \frac{K_1{}^2 T_{6ba}{}^2 v_{Lr}(t_{6a})}{2C_s L_r} = 0. \end{aligned} \tag{12}$$

At end of this interval, the variation of the resonant current can be calculated as

$$\begin{aligned} & \Delta i_{Lr1} \\ & = \frac{K_2{}^2 V_2 \phi + \sqrt{(K_2{}^2 V_2 \phi)^2 + 8C_s L_k{}^2 f_s{}^2 v_{Lr}(t_{6a})^2 / L_r}}{4K_1 L_k f_s}. \end{aligned} \tag{13}$$

Then, the duration T_{6ba} from t_{6a} to t_{6b} can be expressed as

$$T_{6ba} = t_{6b} - t_{6a} = -\frac{2L_k f_s C_s v_{Lr}(t_{6a})}{K_1 (K_2{}^2 V_2 \phi + 2L_k f_s K_1 \Delta i_{Lr1})}. \tag{14}$$

The second duration is from t_{6b} to the time when the discharge/charge process of secondary side is complete at t_{6c}, the secondary side junction capacitor voltage can be calculated as

$$u_{ds\_s}(t_{6b}) = \frac{v_{Cr}}{2K_1} = \frac{V_2}{8RC_r f_s K_1 (K_1 + K_2)}. \tag{15}$$

When v_{Lr} becomes larger than zero, i_{Lr} starts to increase until the discharge/charge process ends. The variation of the resonant current in this interval can be calculated as

$$\Delta i_{Lr2} = \frac{-{K_2}^2 V_2 \phi + \sqrt{\left({K_2}^2 V_2 \phi\right)^2 + 16{L_k}^2 {f_s}^2 C_s u_{ds\_s}(t_{6b}) v_{Cr}/L_r}}{4K_1 L_k f_s}. \tag{16}$$

Then, the duration T_{6cb} from t_{6b} to t_{6c} can be calculated as

$$T_{6cb} = t_{6c} - t_{6b} = -\frac{4L_k f_s C_s u_{ds\_s}(t_{6b})}{K_1\left(-{K_2}^2 V_2 \phi + 2K_1 L_k f_s \Delta i_{Lr1}\right)}. \tag{17}$$

Finally, the total variation of the resonant current Δi_{Lr} and the duration from T_{p_dis} to the completion of the discharge/charge process can be obtained as

$$\begin{cases} \Delta i_{Lr} = \Delta i_{Lr2} - \Delta i_{Lr1} \\ T_{6ca} = T_{6ba} + T_{6cb} \end{cases}. \tag{18}$$

Based on (10) and (18), i_{s_end} can be calculated as

$$i_{s\_\mathrm{end}} = K_1 \Delta i_{Lr} - \frac{{K_2}^2 V_o \phi}{2L_k f_s} + K_2 \frac{V_{C2} + K_2 V_o}{L_k}\left(T_{\mathrm{dead}} - T_{6ca} - T_{p\_\mathrm{dis}}\right) \tag{19}$$

where Δi_{Lr} can be calculated according to (13) and (16), and T_{6ca} can be calculated according to (10), (14), and (17). Therefore, through proper parameter design, the current before the switches turned on, i_{s_end} in (19), can be negative, thus achieving the ZVS operation of the secondary side.

B. ZVS Analysis of LLC Primary Circuit

1) Forward Power Transmission Mode: When the switches of *LLC* primary circuit are turned OFF, the resonant current equals to the magnetizing inductor current. Then, the ZVS realization depends on the magnetizing inductor current i_{Lm}. To complete the discharge/charge process of the junction capacitor during dead time, according to (10), the discharge/charge time can be derived as

$$T_{p\_\mathrm{dis}} = 8C_{p\_LLC} L_m f_s \quad \le T_{\mathrm{dead}}. \tag{20}$$

At the same time, the dead time should not set too large to cause antiresonance.

2) Backward Power Transmission Mode: As shown in Fig. 4(b), under the backward power transmission mode, the charging/discharging energy are also provided by the magnetizing current, therefore, (20) is still valid.

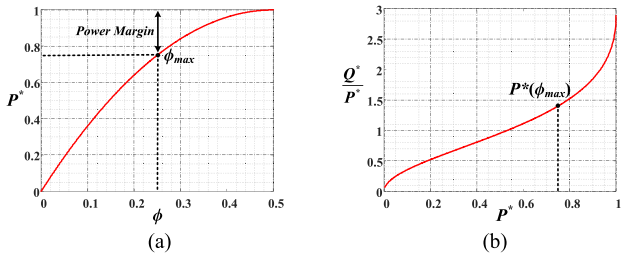

(a) (b)

Fig. 8. Transferred power characteristics and the ratio of the reactive power for the DAB converter. (a) Transferred power characteristics. (b) Ratio of the reactive power to active power.

C. ZVS Analysis of Auxiliary DAB Circuit

The ZVS operation analysis of auxiliary DAB circuit using the SPS modulation strategy has been discussed extensively in the literature. In the proposed converter, the energy stored in the leakage inductor needs to be higher than the energy stored in the junction capacitor of switches, as follow:

$${L_k i_{Lk\_\mathrm{off\,min}}}^2 \ge 2C_{p\_\mathrm{DAB}} {V_{C2}}^2 \tag{21}$$

where i_{Lk_offmin} is the minimum turn OFF current.

IV. Parameters Design

According to the abovementioned analysis, to realize the ZVS operation of all the switches under different power transmission directions, the parameters needs to be proper designed.

A. Power Distribution and Transformer Turns Ratios

Since the proposed converter is a sigma structure, the distribution of power flowing through *LLC* primary circuit, and auxiliary DAB circuit is determined by the corresponding transformer turns ratio. Referring the power distribution analysis in [19], this article further discusses. It can be known that if the power ratio of auxiliary DAB circuit is very small, it will affect the dynamics of the system. At the same time, the power ratio of *LLC* primary circuit will increase accordingly, causing high voltage stress of the switches, which will result in the need for higher voltage level switching devices and insulation. In this article, the power distribution is designed based on the tradeoff between ZVS region and these aforementioned factors, which will be shown in part C.

B. Leakage Inductor L_k

The leakage inductor in auxiliary DAB circuit is a power link between the primary and secondary side, and it is related to the maximum transmission power. The maximum steady-state phase shift angle $\phi_{\max}$ is defined as 0.25 considering the maximum power margin and the ratio of the reactive power to active power, as shown in Fig. 8.

The maximum value of L_k can be obtained as

$$L_k \le \frac{K_2 R V_{C2} \phi_{\max}(1 - \phi_{\max})}{2V_2 f_s}. \tag{22}$$

Then, based on the ZVS operation analysis of auxiliary DAB circuit, the minimum i_{Lk_off} can be deduced according to (3) as

$$i_{Lk\_\mathrm{off\,min}} = \frac{K_2 V_2 \phi_{\min}}{2L_k f_s} = \frac{i_{Lk\_\mathrm{off}}}{n} \tag{23}$$

where n is the ratio between $\phi_{\max}$ and $\phi_{\min}$, which can be obtained as

$$n = \frac{\phi_{\max}}{\phi_{\min}} = \frac{2\phi_{\max}}{1 - \sqrt{1 - (0.8)\,\phi_{\max}\,(1 - \phi_{\max})}}. \tag{24}$$

Substituting (22) and (23) into (24) can obtain as

$$L_k \geq \frac{2C_{p\_\mathrm{DAB}} K_2^2 [nRV_{\mathrm{C2}}\,(1 - \phi_{\max})]^2}{{V_2}^2}. \tag{25}$$

The minimum leakage inductor corresponding to the minimum turn OFF current can be obtained, which ensures ZVS operation under light load conditions (10% of rated power). If the value is less than the rated maximum inductor value, a compromise can be made within the interval, given as

$$\frac{2C_{p\_\mathrm{DAB}} K_2^2 [nRV_{C2}\,(1 - \phi)]^2}{{V_2}^2} \leq L_k \leq \frac{K_2 RV_{C2}\phi\,(1 - \phi)}{2V_2 f_s}. \tag{26}$$

C. Magnetizing Inductor L_m

According to the previous ZVS analysis, the secondary side under backward power transmission is the most difficult to achieve ZVS. The discharge/charge time of *LLC* primary circuit T_{p_dis} is designed to be smaller than the secondary side time T_{s_dis} for extend the ZVS operation range. According to (10), L_m should be satisfied the following relationship:

$$L_m \leq \frac{C_s L_k}{2{K_2}^2 \phi C_{p\_LLC}}. \tag{27}$$

It can be seen from (24) and (25), the magnetizing inductor is related to the transformer turns ratio, which means that to determine the above parameters, it is necessary to determine the power distribution. Since the proposed structure, the power distribution of the auxiliary DAB circuit when ignoring the conversion loss is given as

$$\frac{P_{\mathrm{DAB}}}{P_o} = \frac{P_{\mathrm{DAB}}}{P_{LLC} + P_{DAB}} = \frac{V_{C2} i_1}{V_{C1} i_1 + V_{C2} i_1} = \frac{K_2}{K_1 + K_2} = \lambda \tag{28}$$

where i_1 is input current and λ is a power distribution coefficient. In order to determine the power distribution relationship, the basic parameters of the proposed converter are given in Table I, where the value of the junction capacitors can be obtained by referring to the datasheet. To achieve high efficiency, the proportion of the power that flows through auxiliary DAB circuit should be as low as possible to ensure that main power flows through *LLC* primary circuit. Generally, λ is better smaller than 1/3, thus, the leakage inductor L_k and power devices can be initially determined according to (26). As the switching frequency selects as 100 kHz, the resonant inductor L_r and the resonant capacitor

TABLE I
SYSTEM PARAMETERS

Symbol	Parameter	Value
V_1	Input Voltage	750 V
V_2	Output Voltage	400 V
L_r	Resonant Inductor	25 μH
C_r	Resonant Capacitor	0.1 μF
L_k	Leakage Inductor	55 μH
P_o	Rated Power	2 kW
f_s	Switching Frequency	100 kHz
C_{p_LLC}	Junction Capacitor in LLC Primary Circuit	200 pF
C_{p_DAB}	Junction Capacitor in Auxiliary DAB Circuit	250 pF
C_s	Junction Capacitor in Secondary	290 pF

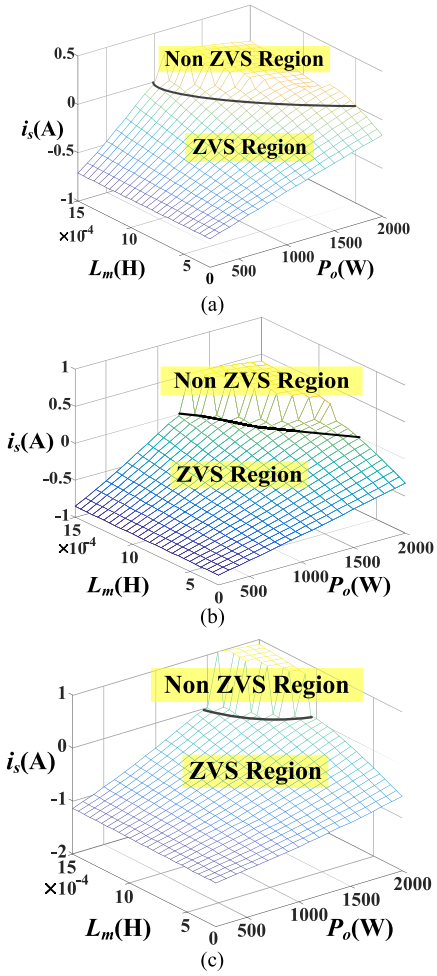

Fig. 9. ZVS range of the secondary side in backward power transmission mode. (a) $\lambda = 1/3$. (b) $\lambda = 4/15$. (c) $\lambda = 1/5$.

C_r are selected, as shown in Table I, to form a resonant tank, where the relationship can be expressed as

$$f_s = f_r = \frac{1}{2\pi\sqrt{L_r C_r}}. \tag{29}$$

In order to final design magnetizing inductor L_m, under the premise of satisfying (27), substituting system parameters into (19) to calculate the secondary side current i_s at the end of dead time under different L_m with different λ, as shown in Fig. 9. If

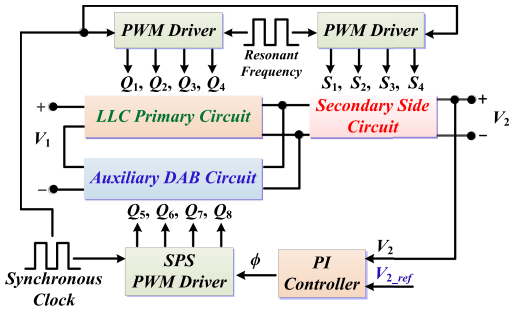

Fig. 10. System control block diagram.

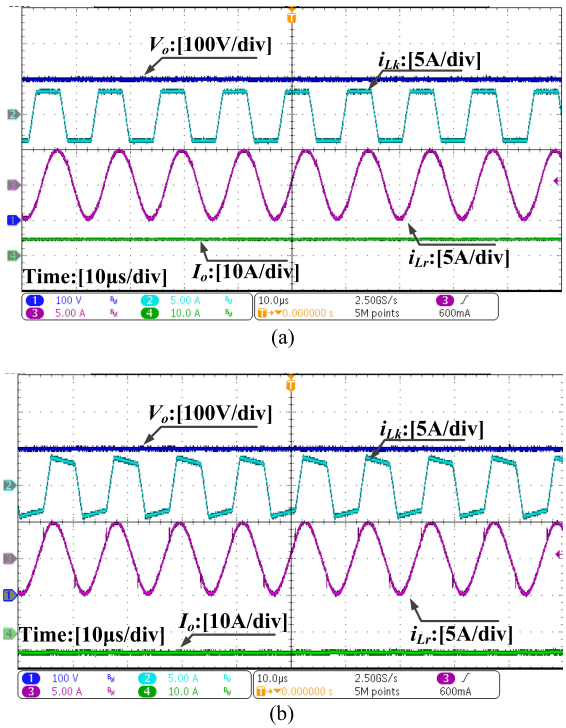

Fig. 11. Performance of the proposed converter under different power transmission modes. (a) Forward power transmission mode. (b) Backward power transmission mode.

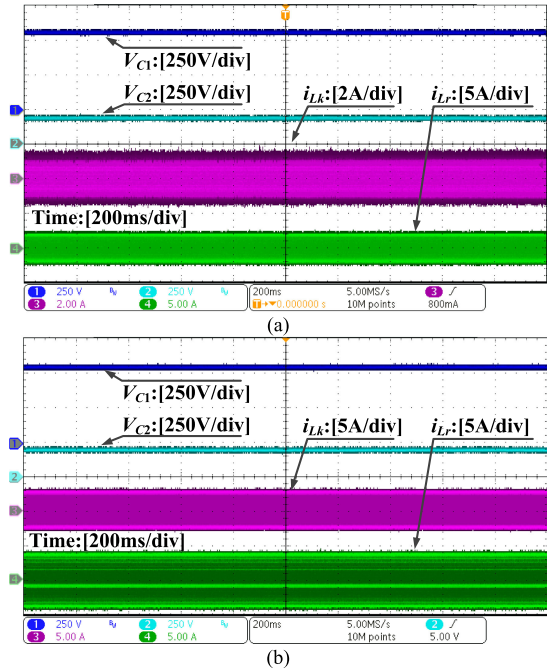

Fig. 12. Key waveforms of power distribution of the proposed converter. (a) Under light load condition. (b) Under full load condition.

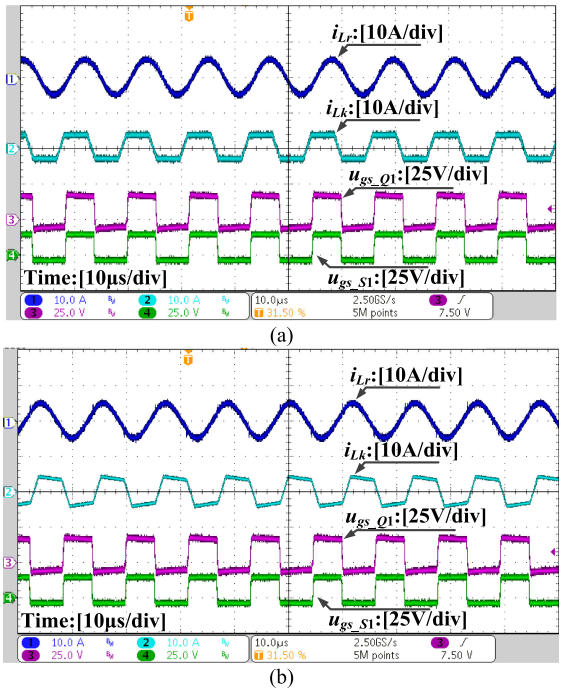

Fig. 13. Gate signals of *LLC* primary circuit and secondary side under the full load condition. (a) Forward power transmission mode. (b) Backward power transmission mode.

the secondary side current i_s can maintain a negative value, the ZVS operation can be achieved. It can be seen from Fig. 9, if L_m exceeds the boundary, there will be a case where i_s is greater than zero in the same power range, thus causing ZVS to be lost. It can also be concluded from Fig. 9 that when λ is decreased, the ZVS region can be extended.

According to previous analysis, the voltage regulation ability will be weak as λ decreases. Finally, the magnetizing inductor L_m and the power distribution coefficient λ are selected as 500 μH and 4/15 for a compromise according to Fig. 9.

V. Experiment Results

A 2 kW *LLC*-DAB bidirectional DCX converter prototype is built up with 750 V input and 400 V output voltage. The system circuit parameters are previously shown in Table I. The system control block diagram is shown in Fig. 10. The *LLC* circuit is open loop operation, which is operated at fixed resonant switching frequency. A proportional-integral controller is adopted by auxiliary DAB circuit to regulate the output voltage regulation, which is implemented on a digital signal processor TMS320F28069.

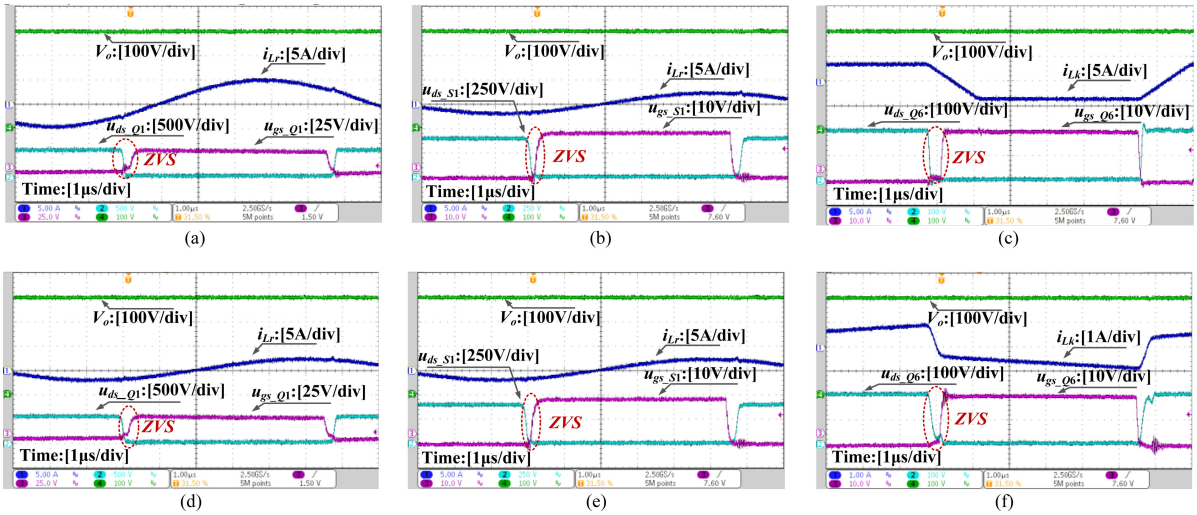

Fig. 14. Soft switching performance of the proposed converter under forward power transmission mode. (a) and (d) are for *LLC* primary circuit in full and light load conditions. (b) and (e) are for the secondary side in full and light load conditions. (c) and (f) are for auxiliary DAB circuit in full and light load conditions.

A. Steady-State Performance

The steady-state performance of the proposed converter under full load in different power transmission directions is shown in Fig. 11, which includes output voltage $V_{\rm o}$, leakage inductor current of auxiliary DAB circuit i_{Lk}, resonant current of *LLC* primary circuit i_{Lr} and output current I_o, respectively.

In order to verify the power distribution relationship, Fig. 12 shows the input voltage of *LLC* primary circuit and auxiliary DAB circuit, V_{C1} and V_{C2}, under light and full load condition. It can be seen that the ratio of input voltage of *LLC* primary circuit and auxiliary DAB circuit is around 550/200. As the proposed converter is series-connected at the input, the input currents of the two circuits are equal. Hence, it can be calculated that the power flowing through *LLC* is 550/(550+200) = 73.3% of the total power, and the power flowing through DAB accounts for 200/(550+200) = 26.7% of the total power. Therefore, the main power is processed by *LLC* primary circuit, while partial power has been transferred through the auxiliary DAB circuit. This agrees well with the analysis.

Fig. 13 shows the gate signals of the switches in *LLC* primary circuit (u_{gs_Q1}) and the secondary side (u_{gs_S1}) under the forward and backward power transmission modes, which are consistent. It means that the PWM scheme does not need to be changed when the power direction changes, and it is easy to implement.

B. Soft Switching Performance and Comparison

In order to verify ZVS performance under the forward power transmission mode. The soft switching performance of proposed solution is shown in Fig. 14, where Fig. 14(a)–(e) shows the output voltage $V_{\rm o}$, resonant current of *LLC* primary circuit i_{Lr}, drain to source voltage, and drive voltage can be observed. Fig. 14(c) and (f) shows the output voltage $V_{\rm o}$, leakage current of auxiliary DAB circuit i_{Lk}, drain to source voltage and drive voltage, respectively. From the measured waveforms, the ZVS operation on all switches of the *LLC* primary circuit, secondary side and auxiliary DAB circuit can be realized under the full load (2 kW) and light load (200 W).

TABLE II
SWITCH TYPES FOR THE CONVERTERS

Item	Proposed Converter	Converter in [19]
Q_1 - Q_4	NTHL190N65S3HF	
S_1 - S_4	FCH072N60	IPW60R170CFD7
Q_5 - Q_8	IRFP4137PBF	
S_5 - S_8	Not Used	IPW60R125P6

Similarly, the soft switching performance under backward power transmission mode is shown in Fig. 15. It can be seen that the ZVS operation on all switches can also be achieved under full load (2 kW) and light load (200 W) condition.

To further demonstrate the superiority of the proposed converter in terms of ZVS operation, comparison experiments are carried out on the traditional DAB-*LLC* DCX converter proposed in [19], where the system parameters are the same as those in Table I, and the switching devices on the secondary side are chosen to be the same, as shown in Table II. Fig. 16 shows its soft switching performance. It can be seen that the ZVS operation is lost at half load and full load conditions when the power transfers backward. Therefore, it can also be verified that under the same modulation strategy, the traditional DAB-*LLC* DCX converter is difficult to completely realize the ZVS operation in full load range under different power transmission modes. While the proposed solution is effective which has been shown in Figs. 14 and 15, respectively.

C. Dynamic Performance and Efficiency

In order to verify the voltage regulation capability, the load is changed from 400 W to 1800 W. The key waveforms are shown in Fig. 17. It can be seen that the output voltage remains stable at 400 V under the load step change.

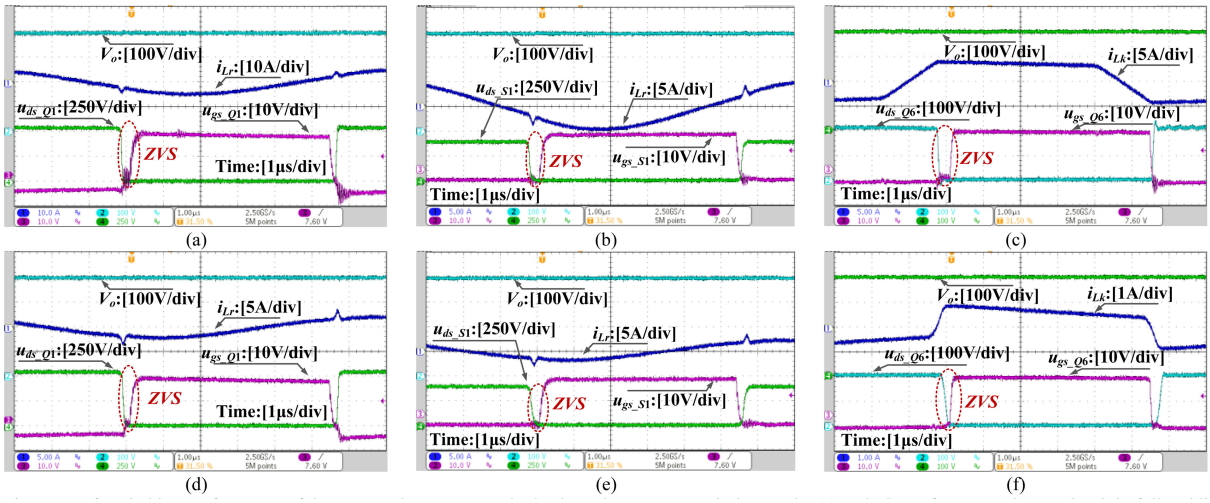

Fig. 15. Soft switching performance of the proposed converter under backward power transmission mode. (a) and (d) are for *LLC* primary circuit in full and light load conditions. (b) and (e) are for the secondary side in full and light load conditions. (c) and (f) are for auxiliary DAB circuit in full and light load conditions.

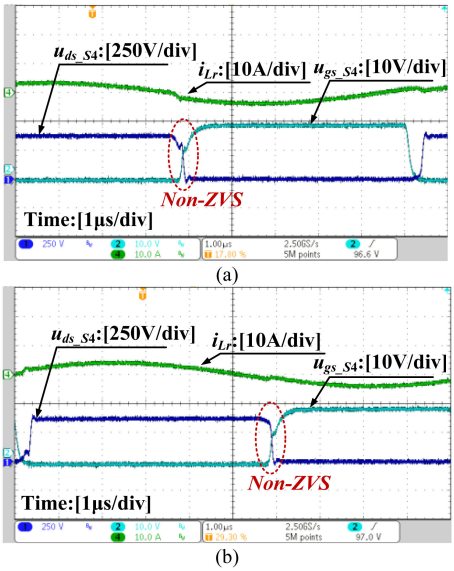

Fig. 16 . Soft switching performance of secondary side in the traditional DAB-*LLC* DCX converter under backward power transfer. (a) Half load condition. (b) Full load condition.

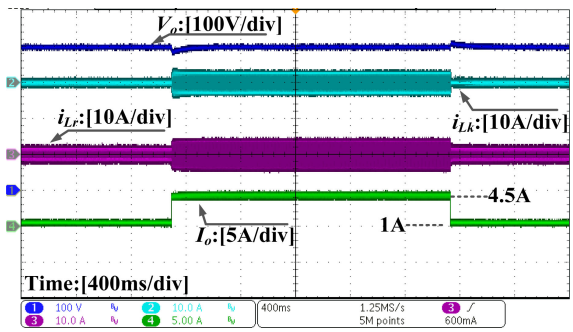

Fig. 17. Dynamic performance of the proposed converter with a load step change.

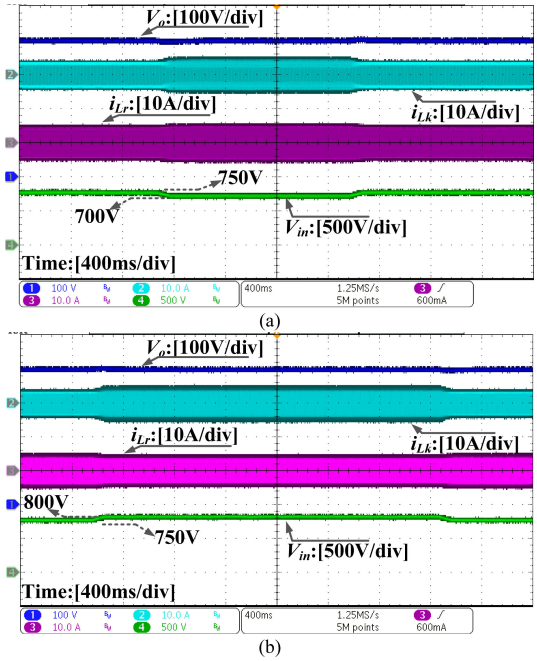

Fig. 18. Performance of the proposed converter with input voltage variation. (a) Input voltage drops. (b) Input voltage increases.

Since *LLC* primary circuit and the secondary side is used as a DCX in the proposed converter, its output voltage is determined by the input voltage. When the input voltage changes, the proposed converter can stabilize the output voltage by adjusting the phase shift angle in auxiliary DAB circuit. Fig. 18 shows the key waveforms when the input voltage drops from 750 V to 700 V and increases from 750 V to 800 V. It can be seen that the output voltage remains constant under different input voltage.

D. Efficiency Comparison

In order to verify the advantages of choosing *LLC* circuit as the main power processing unit, Fig. 19 shows the loss comparison

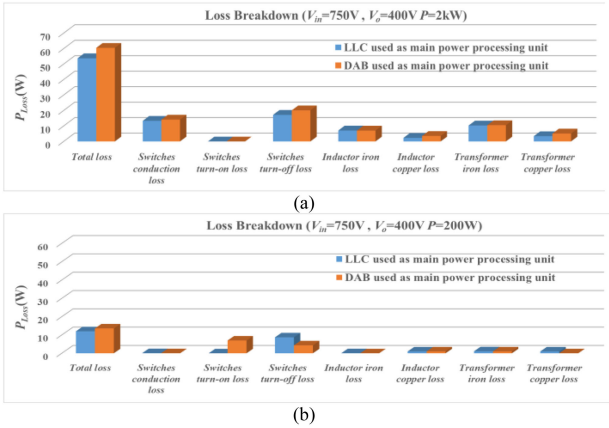

Fig. 19. Comparisons of the calculated power loss breakdown. (a) Under rated power (2 kW). (b) Under light load power (200 W).

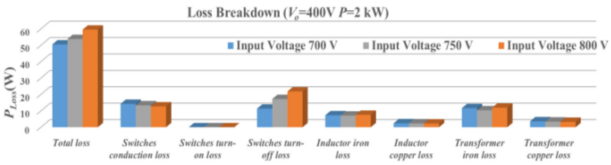

Fig. 20. Loss breakdown results of the proposed converter under the different input voltage.

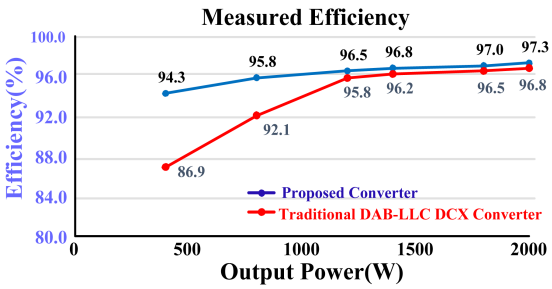

Fig. 21. Measured efficiency under different load conditions.

between the proposed converter with *LLC* as the main power processing unit and the proposed converter with DAB as the main power processing unit, under rated power (2 kW) and light load power (200 W), respectively. It can be seen that compared with DAB as the main power processing unit under rated power and light power, the loss reduction of the proposed converter is 6.8 W and 1.6 W, respectively. Therefore, the proposed converter with *LLC* as the main power processing unit is more efficiency.

For better illustrating the efficiency performance of the proposed converter within a certain input voltage range, the comparison of loss breakdown results are presented in Fig. 20 when the input voltage are 700 V, 750 V, and 800 V, respectively. It can be seen that when the input voltage is increased, the total loss are increased. That is because the power flowing through the DAB circuit is increased, resulting in increased loss. However, the increased loss is relatively small and acceptable.

The comparisons of the measured efficiency under different load conditions between the proposed converter and the traditional DAB-*LLC* DCX converter are shown in Fig. 21. It can be seen that the peak efficiency of the proposed converter is 97.3%. The efficiency of the traditional converter under light load is much smaller, and the efficiency under other loads is also smaller than the proposed converter. In addition, the proposed converter also has less switch number compared with the traditional converter.

VI. Conclusion

To achieve flexible voltage regulation, and a wide load range of ZVS operation of all switches under the forward and backward power transmission, this article proposed an *LLC*-DAB bidirectional DCX converter. The proposed converter adopts a sigma structure. By connecting to the same full-bridge circuit in the secondary side, the proposed converter requires four fewer switches than the conventional solution. In this way, DAB is used as an auxiliary power regulation unit that only processes partial power, and *LLC* primary circuit transfers the main power with a simple PWM scheme, achieving a high efficiency. The operation modes, the ZVS operation range considering the switch junction capacitors, and the design are discussed in detail. Finally, the experimental results have verified the effectiveness of the proposed converter by comparing its performance with that of the conventional solution. As for the future work, since the outputs of the two transformers are connected together, the modeling of this structure to analyze the dynamic performance is worth of study.

References

[1] M. Fariborz, M. Craciun, D. S. Gautam, W. Eberle, and W. G. Dunford, "An LLC resonant DC–DC converter for wide output voltage range battery charging applications," *IEEE Trans. Power Electron.*, vol. 28, no. 12, pp. 5437–5445, Dec. 2013.

[2] C. Wang, S. Zhang, Y. Wang, B. Chen, and J. Liu, "A 5-kW isolated high voltage conversion ratio bidirectional CLTC resonant DC–DC converter with wide gain range and high efficiency," *IEEE Trans. Power Electron.*, vol. 34, no. 1, pp. 340–355, Jan. 2019.

[3] G. Ortiz, M. Leibl, J. Huber, and J. W. Kolar. "Design and experimental testing of a resonant DC-DC converter for solid-state transformers," *IEEE Trans. Power Electron.*, vol. 32, no. 10, pp. 7534–7542, Oct. 2017.

[4] G. Li and X. Wu, "A high power density 48V-12V DCX with 3-D PCB winding transformer," in *Proc. IEEE Appl. Power Electron. Conf. Expo.*, 2020, pp. 463–467.

[5] X. Chen *et al.*, "A natural bidirectional input-series-output-parallel LLC-DCX converter with automatic power sharing and power limitation capability for li-ion battery formation and grading system," *IEEE J. Emerg. Sel. Topics Power,* vol. 8, no. 4, pp. 3618–3632, Dec. 2020.

[6] C. Yeh, L. Zhang, J. Choe, C. Chen, O. Yu, and J. Lai. "Light-load efficiency improvement for LLC converter with synchronous rectification in solid-state transformer application," in *Proc. IEEE Appl. Power Electron. Conf. Expo.*, 2018, pp. 2142–2147.

[7] H. Chen and X. Wu, "LLC resonant DC transformer (DCX) with parallel PWM output tight regulation," in *Proc. IEEE Energy Convers. Congr. Expo.*, 2014, pp. 4742–4747.

[8] J. Sun, M. Xu, D. Reusch, and F. C. Lee, "High efficiency quasi-parallel voltage regulators," in *Proc. IEEE Appl. Power Electron. Conf. Expo.*, 2008, pp. 811–817.

[9] M. Ahmed, C. Fei, F. C. Lee, and Q. Li, "Single-stage high-efficiency 48/1V sigma converter with integrated magnetics," *IEEE Trans. Ind. Electron.*, vol. 67, no. 1, pp. 192–202, Jan. 2020.

[10] Y. Liu, X. Chen, Y. Wu, K. Yang, J. Zhu, and B. Li, "Enabling the smart and flexible management of energy prosumers via the energy router with parallel operation mode," *IEEE Access*, vol. 8, pp. 35038–35047, Feb. 2020.

[11] X. Wu, H. Chen, and Z. Qian, "1-MHz LLC resonant DC transformer (DCX) with regulating capability," *IEEE Trans. Ind. Electron.*, vol. 63, no. 5, pp. 2904–2912, May 2016.
[12] T. Liu, X. Wu, and S. Yang, "1 MHz 48V-12V regulated DCX with single transformer," *IEEE J. Emerg. Sel. Topics Power*, vol. 9, no. 1, pp. 38–47, Feb. 2021.
[13] D. Sha; X. Wang and D. Chen, "High-efficiency current-fed dual active bridge DC–DC converter with ZVS achievement throughout full range of load using optimized switching patterns," *IEEE Trans. Power Electron.*, vol. 33, no. 2, pp. 1347–1357, Feb. 2018.
[14] G. Xu, L. Li, X. Chen, Y. Liu, Y. Sun, and M. Su, "Optimized EPS control to achieve full load range ZVS with seamless transition for dual active bridge converters," *IEEE Trans. Ind. Electron.*, vol. 68, no. 9, pp. 8379–8390, Sep. 2021.
[15] S. Mukherjee, A. Kumar, and S. Chakraborty, "Comparison of DAB and LLC DC–DC converters in high-step-down fixed-conversion-ratio (DCX) applications," *IEEE Trans. Power Electron.*, vol. 36, no. 4, pp. 4383–4398, Apr. 2021.
[16] B. Zhao, Q. Song, W. Liu, and Y. Sun "Overview of dual-active-bridge isolated bidirectional DC–DC converter for high-frequency-link power-conversion system," *IEEE Trans. Power Electron.*, vol. 29, no. 8, pp. 4091–4106, Aug. 2014.
[17] Y. Sun, Z. Gao, C. Wu, and Z. Chen, "A hybrid modular DC solid-state transformer combining high efficiency and control flexibility," *IEEE Trans. Power Electron.*, vol. 35, no. 4, pp. 3434–3448, Apr. 2020.
[18] J. Yao, W. Chen, C. Xue, and T. Wang, "An ISOP hybrid DC transformer combining multiple SRCs and DAB converters to interconnect MVDC and LVDC distribution converters," *IEEE Trans. Power Electron.*, vol. 35, no. 11, pp. 11442–11452, Nov. 2020.
[19] Y. Liao *et al.*, "Single-stage DAB-LLC hybrid bidirectional converter with tight voltage regulation under DCX operation," *IEEE Trans. Ind. Electron.*, vol. 68, no. 1, pp. 293–303, Jan. 2020.
[20] J. Xu *et al.*, "PWM modulation and control strategy for LLC-DCX converter to achieve bidirectional power flow in facing with resonant parameters variation," *IEEE Access*, vol. 7, pp. 54693–54704, May 2019.
[21] J. Zhang, J. Liu, J. Yang, N. Zhao, Y. Wang, and T. Q. Zheng, "An LLC-LC type bidirectional control strategy for an LLC resonant converter in power electronic traction transformer," *IEEE Trans. Ind. Electron.*, vol. 65, no. 11, pp. 8595–8603, Nov. 2018.
[22] L. Zhu, H. Bai, L. Brown, and M. McAmmond, "Design a 400V-12V 6kW bidirectional auxiliary power module for electric or autonomous vehicles with fast pre-charge dynamics and zero DC bias current," *IEEE Trans. Power Electron.*, vol. 36, no. 5, pp. 5323–5335, May 2021.
[23] H. Wu, S. Ding, K. Sun, L. Zhang, Y. Li, and Y. Xing, "Bidirectional soft-switching series-resonant converter with simple PWM control and load-independent voltage-gain characteristics for energy storage system in DC microgrids," *IEEE J. Emerg. Sel. Topics Power*, vol. 5, no. 3, pp. 995–1007, Sep. 2017.
[24] H. Li, Z. Zhang, S. Wang, J. Tang, X. Ren, and Q. Chen. "A 300-kHz 6.6-kW SiC bidirectional LLC onboard charger," *IEEE Trans. Ind. Electron.*, vol. 67, no. 2, pp. 8595–8604, Feb. 2020.
[25] T. Jiang, J. Zhang, X. Wu, K. Sheng, and Y. Wang, "A bidirectional LLC resonant converter with automatic forward and backward mode transition," *IEEE Trans. Power Electron.*, vol. 30, no. 2, pp. 757–770, Feb. 2015.
[26] C. Chen, X. Zhao, C. Yeh, and J. Lai, "Analysis of the zero-voltage switching condition in LLC series resonant converter with secondary parasitic capacitors," in *Proc IEEE Appl. Power Electron. Conf. Expo.*, 2019. pp. 828–832.
[27] D. Costinett, D. Masksimovic, and R. Zane, "Circuit-oriented treatment of nonlinear capacitances in switched-mode power supplies," *IEEE Trans. Power Electron.*, vol. 30, no. 2, pp. 985–995, Feb. 2015.

Yuefeng Liao (Student Member, IEEE) was born in Jishou, China, in 1988. He received the B.S. degree in control theory and control engineering from Harbin Engineering University, Harbin, China, in 2013. He is currently working toward the Ph.D. degree with Central South University, Changsha, China.

His research interests include modeling of dc–dc resonant converters, controller design in power electronic, and topology research.

Guo Xu (Senior Member, IEEE) received the B.S. degree in electrical engineering and automation and the Ph.D. degree from the Beijing Institute of Technology, Beijing, China, in 2012 and 2018, respectively.

From 2016 to 2017, he was a Visiting Student with the Center for Power Electronics System, Virginia Polytechnic Institute and State University, Blacksburg, VA, USA. Since 2018, he has been with the School of Automation, Central South University, Changsha, China, where he is currently an Associate Professor.

His research interests include modeling and control of power electronics converters, high-efficiency power conversion, and magnetic integration in power converters.

Tao Peng (Member, IEEE) was born in Hunan, China, in 1965. She received the B.S. degree in industrial electric automation from the Hunan University of Technology, Zhuzhou, China, in 1991, the M.S. degree in detection instrument and meter from the National University of Defense Technology, Changsha, China, in 1991, and the Ph.D. degree in control science and engineering from the Central South University, Changsha, China, in 2005.

From 2004 to 2010, she was a Professor with the Hunan University of Technology. Since 2010, she has been a Professor with the School of Automation, Central South University. Her research interests include fault diagnosis and tolerant control for power electronic devices and systems, control theory, and application.

Yao Sun (Member, IEEE) received the B.S., M.S., and Ph.D. degrees from the School of Information Science and Engineering, Central South University, Changsha, China, in 2004, 2007, and 2010, respectively.

He is currently with the School of Automation, Central South University, China, as a Professor. His research interests include matrix converter, microgrid, and wind energy conversion system.

Dong Liu (Senior Member, IEEE) received the B.Eng. and M.Sc. degrees in electrical engineering from South China University of Technology, Guangzhou, China, in 2008 and 2011, respectively, and the Ph.D. degree in energy technology from the Department of Energy Technology, Aalborg University, Aalborg, Denmark, in 2018.

From 2018 to 2021, he was a Postdoctoral Researcher with the Department of Energy Technology, Aalborg University. He is currently with the Department of Electronic and Electrical Engineering, University of Sheffield as a Research Associate. From 2011 to 2014, he was an R&D engineer in Emerson Network Power Co., Ltd., Shenzhen, China. From May 2017 to November 2017, he was a Visiting Scholar with the Center for Power Electronics Systems, Virginia Tech, Blacksburg, VA, USA. His main research interests include the modeling and control of power electronics converters, high-efficiency power conversion systems, and power electronics applications in renewable energy power generations.

Yongheng Yang (Senior Member, IEEE) received the B.Eng. degree in electrical engineering and automation from Northwestern Polytechnical University, Xi'an, China, in 2009, and the Ph.D. degree in energy technology (power electronics and drives) from Aalborg University, Copenhagen, Denmark, in 2014.

He was a postgraduate student with Southeast University, China, from 2009 to 2011. In 2013, he spent three months as a Visiting Scholar with Texas A&M University, USA. Since 2014, he has been with the Department of Energy Technology, Aalborg University, where he became a tenured Associate Professor in 2018. In January 2021, he was with Zhejiang University, China, where he is currently a ZJU100 Professor with the Institute of Power Electronics, College of Electrical Engineering. His current research interests include the grid-integration of photovoltaic systems and control of power converters, in particular, the mechanism and control of grid-forming power converters and systems.

Dr. Yang was the Chair of the IEEE Denmark Section (2019–2020). He is an Associate Editor for several IEEE Transactions/Journals. He is a Deputy Editor of the *IET Renewable Power Generation for Solar Photovoltaic Systems*. He was the recipient of the 2018 IET Renewable Power Generation Premium Award and was an Outstanding Reviewer for the IEEE TRANSACTIONS ON POWER ELECTRONICS in 2018. He was the recipient of the 2021 Richard M. Bass Outstanding Young Power Electronics Engineer Award from the IEEE Power Electronics Society. In addition, he has received two IEEE Best Paper Awards. He is currently the Secretary of the IEEE Power Electronics Society Technical Committee on Sustainable Energy Systems.

Mei Su was born in Hunan, China, in 1967. She received the B.S., M.S., and Ph.D. degrees from the School of Information Science and Engineering, Central South University, Changsha, China, in 1989, 1992, and 2005, respectively.

Since 2006, she has been with the School of Automation, Central South University, Changsha, China. Her research interests include matrix converter, adjustable speed drives, and wind energy conversion system.